Dalton Transactions

ROYAL SOCIETY OF CHEMISTRY

COMMUNICATION

View Article Online
View Journal | View Issue

Cite this: *Dalton Trans.*, 2022, **51**, 7783

Received 31st March 2022,
Accepted 29th April 2022

DOI: 10.1039/d2dt00991a

rsc.li/dalton

Dehydration-activated structural phase transition in a two-dimensional hybrid double perovskite†

Rui-Ying Ren,‡[a] Chang-Yuan Su, *‡[a,b] Ting Shao,[a] Zhi-Xu Zhang,[b] Pei-Zhi Huang,[a] Yi Zhang,[b] Qiang-Qiang Jia*[a] and Da-Wei Fu *[a]

As a feasible lead-free scheme, organic–inorganic hybrid double perovskites show many excellent properties, including ferroelectricity, ferroelasticity, self-powered circularly polarized light detection and so on. In this work, the solid-to-solid structural phase transition of a two-dimensional hybrid double perovskite $(CHA)_4CuBiI_8$ was successfully activated *via* the dehydration of $(CHA)_4CuBiI_8{\cdot}H_2O$, which was proven by differential scanning calorimetry (DSC) and temperature-dependent dielectric measurements. Using variable-temperature single-crystal X-ray diffractometry, the cause behind the phase transition of $(CHA)_4CuBiI_8$ was determined to be the overall coordination of distortion and movement of the inorganic skeleton and thermal deformation of the cationic structure. In addition, the substance after dehydration shows good stability in multiple reversible switching during dielectric tests. The interesting dehydration-activated results of the material contribute towards a further expansion of the properties and potential application of hybrid double perovskites.

Introduction

The wonderful electronic and optical properties and other physical properties of lead halide hybrid perovskites represented by $CH_3NH_3PbI_3$ have made them a hot research topic. Based on their properties, many applications, including solar cells,[1–5] lasers,[6–8] detectors,[9–11] information storage,[1,12–16] light-emitting diodes[17–19] and so on,[20,21] have been achieved using these materials. However, on account of their toxicity and long-term instability, lead-based materials seriously affect the health of animals and plants, thus hindering their practical application[22] and meaning that the research on lead-free perovskites has become an important research hotspot.[23–25] Homo-valent replacement, as a popular lead-free solution using Ge and Sn, can be used to construct lead-free perovskites that show superior optical and electronic properties.[26–28] However, Ge- and Sn-based perovskites have still been criticized for their instability, prompting scientists to attempt hetero-valent replacement to produce materials with chemical stability.[29–32]

In order to maintain charge neutrality, hetero-valent replacement can be divided into two subcategories, namely ion-splitting ($A_2B^IB^{III}X_6$) and vacancy ordering ($A_3\square B^{III}X_9$ and $A_2\square B^{IV}X_6$, where □ is a vacancy), where the B^I-site cation can be an alkali metal and group IB elements, the B^{III}-site cation is an element in groups A or B, and X at the corner is a halogen, CN^- or NO_3^-, according to current knowledge.[28,30,31,33–36] The various possible combinations that are achievable make hetero-valent replacement schemes diverse compared to traditional single metal hybrid materials.[28,31,33,37] As ion-splitting double perovskites, two-dimensional double perovskites ($A_4B^IB^{III}X_8$) possess multiple attractive physical properties, including X-ray detection,[38,39] ferroelectricity,[38,40] photoluminescence,[41,42] obvious light-response behavior,[30,43–45] and other characteristics,[46,47] which prompted us to explore the other physical properties of double perovskites. Among double perovskites, ones with solid-to-solid phase transition are extremely rare. The reason for this situation is the difficulty in synthesizing hybrid double perovskites, including the formation of low-dimensional multiple competitive phases, complex synthesis methods and so on.[30,42,48,49]

Crystal dehydration refers to the removal of crystal water from crystals, which plays an important role in some fields. For example, after protein crystals are dehydrated, the diffraction quality of the macromolecular crystals improves.[50] In

[a]*Institute for Science and Applications of Molecular Ferroelectrics, Key Laboratory of the Ministry of Education for Advanced Catalysis Materials, Zhejiang Normal University, Jinhua, 321004, People's Republic of China. E-mail: scywmy@163.com, jiaqq_zbdx@163.com, dawei@zjnu.edu.cn*

[b]*Ordered Matter Science Research Center, Jiangsu Key Laboratory for Science and Applications of Molecular Ferroelectrics, Southeast University, Nanjing, 211189, People's Republic of China*

†Electronic supplementary information (ESI) available: Fig. S1–S5, Table S1–S6. CCDC 2167267 ($(CHA)_4CuBiI_8{\cdot}H_2O$ at 150 K), 2120152 ($(CHA)_4CuBiI_8$ at 400 K) and 2120153 ($(CHA)_4CuBiI_8$ at 150 K). For ESI and crystallographic data in CIF or other electronic format see DOI: **https://doi.org/10.1039/d2dt00991a**

‡The authors contributed equally to this work.

addition, in hybrid materials containing Ni, Co, Dy and other elements, such materials may undergo metamagnetic behavior after dehydration.[51–53] In this work, we developed a dehydration-activated phase transition material, marking an important contribution in solid-to-solid structural phase transition materials.

Firstly, according to the published three solid-to-solid phase transition substances $(CHA)_2CdCl_4$,[54] $(CHA)_2PbBr_{4-4x}I_{4x}$[55] and $(CHA)_2BiCl_5$[56] shown in Table S1 in the ESI,† flexible CHA (CHA = cyclohexanaminium) was selected as an organic template and hybrid double perovskite $(CHA)_4CuBiI_8{\cdot}H_2O$, the construction of which is shown in Scheme 1.[42] As an example of a <100>-oriented Ruddlesden–Popper double perovskite with n = 1, $(CHA)_4CuBiI_8{\cdot}H_2O$ has ideal layer spacing and twisted octahedra, which may endow it with the properties of solid-to-solid structural phase transition. This encouraged us to explore whether $(CHA)_4CuBiI_8{\cdot}H_2O$ has phase transition or other such physical properties (Scheme 1). By means of differential scanning calorimetry (DSC) and variable-temperature single-crystal X-ray diffractometry, $(CHA)_4CuBiI_8{\cdot}H_2O$ was proven to transform into the solid-to-solid structural phase transition material $(CHA)_4CuBiI_8$ after dehydration, and the reason for the phase transition is the overall coordination between distortion and movement of the inorganic skeleton and thermal deformation of the cationic structure. Consistent with the DSC results, $(CHA)_4CuBiI_8$ shows a stable reversible step-like change in its dielectric constant according to the change in temperature, which makes it possible to be potentially used in high-temperature warning devices.

Experimental

Materials

All reagents and solvents mentioned in this work were purchased from commercial suppliers and were not further purified.

Synthesis of $(CHA)_4CuBiI_8{\cdot}H_2O$

A PTFE reaction kettle containing hydroiodic acid (55–58% w/w in H_2O, 5 ml), cyclohexylamine (4 mmol), Bi_2O_3 (0.5 mmol) and CuI (1 mmol) was heated at 403 K for 20 h, and after 24 h of heating was allowed to cool to room temperature to obtain single crystals. The single crystals were then suction filtered with petroleum ether and dried under vacuum. The single crystals obtained were black opaque prisms (yield: *ca.* 85% based on Bi).

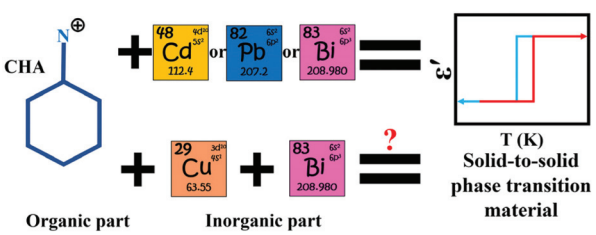

Scheme 1 Motivation for the development of a hybrid double perovskite phase transition material: single metal hybrid phase transition materials based CHA cation.

Dehydration of $(CHA)_4CuBiI_8{\cdot}H_2O$

In order to obtain single crystal of $(CHA)_4CuBiI_8$, $(CHA)_4CuBiI_8{\cdot}H_2O$ needs to be heated at 400 K under the protection of nitrogen to prevent oxidation or other problems. It should be noted that in order to prevent crystal cracking, the heating rate needs to be adjusted to 5 K min^{-1} or even lower. Measured and simulated powder X-ray diffraction patterns of $(CHA)_4CuBiI_8{\cdot}H_2O$ and $(CHA)_4CuBiI_8$ at room temperature can be found in Fig. S1 in the ESI.†

Results and discussion

Thermal analyses

The hybrid double perovskite $(CHA)_4CuBiI_8{\cdot}H_2O$ was successfully synthesized *via* a hydrothermal method. For perovskites, it is necessary to analyze their thermodynamic parameters, so DSC measurements were performed. During the initial heating, only one broad peak near 380 K was observed (Fig. 1a), which corresponds to the loss of crystalline water from the structure, consistent with the thermogravimetric analysis (TGA) results shown in Fig. S2 in the ESI.† In the following two cycles, the exothermic peak at 397 K and the endothermic peak at 404 K appeared stably, implying the occurrence of a reversible solid-to-solid phase transition. For convenience, we labeled the high-temperature phase as phase α and the low-temperature phase as phase β after dehydration.

Variable-temperature crystal structure analysis

Generally speaking, the relationship between the change in the physical properties and the variation in the structure is

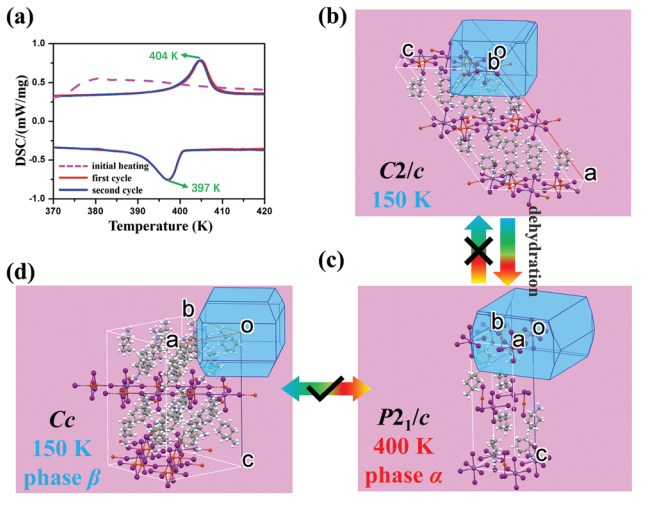

Fig. 1 (a) DSC of initial heating, and first and second cycles. (b–d) Morphology of $(CHA)_4CuBiI_8{\cdot}H_2O$ at 150 K, $(CHA)_4CuBiI_8$ as α (400 K) and β (150 K) phases.

inseparable, so variable-temperature single crystal X-ray diffractometry was carried out to study the structure of $(CHA)_4CuBiI_8{\cdot}H_2O$ at 150 K and $(CHA)_4CuBiI_8$ as α (400 K) and β (150 K) phases.

As shown in Fig. 1b, $(CHA)_4CuBiI_8{\cdot}H_2O$ is in the monoclinic space group $C2/c$ (No. 15) with the cell parameters a = 32.3199 (9) Å, b = 8.5589(3) Å, c = 19.6321(5) Å, β = 125.1470(10)° and V = 4440.5(2) Å^3 (Table S2, ESI†). Due to the use of monoammonium cations instead of diammonium cations, $(CHA)_4CuBiI_8{\cdot}H_2O$ forms a typical <100>-oriented layered Ruddlesden–Popper (RP) type double perovskite with n = 1 like $(APP/AMP)_4AgBiI_8{\cdot}H_2O$[49] and $(COA)_4CuBiI_8$[42] rather than Dion–Jacobson (DJ) type ones like $(3AMPY)_2AgBiI_8{\cdot}H_2O$,[29] $(CHDA)_2CuBiI_8{\cdot}0.5H_2O$[30] and $(MDPA)_2CuBiI_8$.[42] After dehydration, $(CHA)_4CuBiI_8$ crystallizes in $P2_1/c$ (No. 14) at 400 K (Fig. 1c), where a = 9.313(3) Å, b = 9.211(4) Å, c = 26.573(10) Å, β = 91.149(6)° and V = 2279.0(15) Å^3 (Table S2, ESI†). With a decrease in temperature for $(CHA)_4CuBiI_8$, Cc (No. 9) is adopted and the cell parameters are a = 18.7108(11) Å, b = 17.4002(11) Å, c = 26.3343(16) Å, β = 90.686(3)° at 150 K. Compared with the structure at 400 K, the volume of $(CHA)_4CuBiI_8$ at 150 K increases nearly four-fold from 2279.0 (15) Å^3 to 8573.1(9) Å^3 (Fig. S3, ESI†). Besides this, the morphologies of $(CHA)_4CuBiI_8{\cdot}H_2O$ at 150 K and $(CHA)_4CuBiI_8$ in the α (400 K) and β (150 K) phases were explored using Mercury, as shown in Fig. 1b–d, to observe the crystal morphology and structural changes.

In order to better observe the structural changes, the cationic structure and inorganic basic unit before and after dehydration at different temperatures were explored, as shown in Fig. 2. Looking at the cations from front and side views, one can see that the cyclohexanaminium cation undergoes obvious structural deformation in the high-temperature α phase (Fig. 2b) compared with the low-temperature structure (Fig. 2c) for $(CHA)_4CuBiI_8$, suggesting the thermal distortion of molecules at high temperature. It can be observed that there was no significant change in the cations before (Fig. 2a) and after (Fig. 2c) dehydration at a low temperature of 150 K, indicating that dehydration does not change the organic part, but changes the inorganic part, as discussed below.

For the inorganic basic unit of $(CHA)_4CuBiI_8{\cdot}H_2O$ at 150 K (Fig. 2d), the BiI_6 octahedron is slightly distorted, with Bi–I bond lengths ranging from 3.0587(2) Å to 3.1059(2) Å. However, due to the splitting of Cu^- and the large difference in bond lengths of 2.459(6)–3.479(10) Å from average Cu–I bond lengths of 2.65 Å in CuI_3X (X = donors),[57,58] the CuI_6 octahedron is so deformed that it presents an isosceles trapezoid shape when viewed from the direction perpendicular to the two-dimensional plane (Fig. 2d). For $(CHA)_4CuBiI_8$ at 400 K (Fig. 2e) and 150 K (Fig. 2f), the inorganic part has obvious changes in terms of Cu^- and Cu–I bond lengths. Combined with the discussion of the organic part above (Fig. 2b and c), it is not difficult to see that the reason for the phase transition of $(CHA)_4CuBiI_8$ can be attributed to the overall coordination of distortion and movement of the inorganic skeleton and the thermal deformation of cationic structure. Other cell parameters, crystal information, structure refinements, selected bond lengths and bond angles of the different phases are shown in Fig. S3, Tables S3–S5, ESI.†

In addition, packing diagrams including the detailed parameters of $(CHA)_4CuBiI_8{\cdot}H_2O$ at 150 K and $(CHA)_4CuBiI_8$ in the α and β phases are shown in Fig. 3a–c, respectively. From low temperature (150 K) before dehydration to high temperature (400 K) after dehydration, due to the removal of crystal water, the distance between same metal ions in the inorganic skeleton decreases significantly. In the case of global thermal vibration aggregation, the interlayer distance of the two-dimensional structure increases slightly from 13.21 Å to 13.28 Å. With a decrease in temperature from the α to β phase, the interlayer distance of compound **1** after dehydration decreases by 0.11 Å. The results of the above discussion on distance are also reflected in the interaction force between the cations and anions, as shown in Fig. S4 and Table S6 in the ESI.† Observing the inorganic skeleton from the direction perpen-

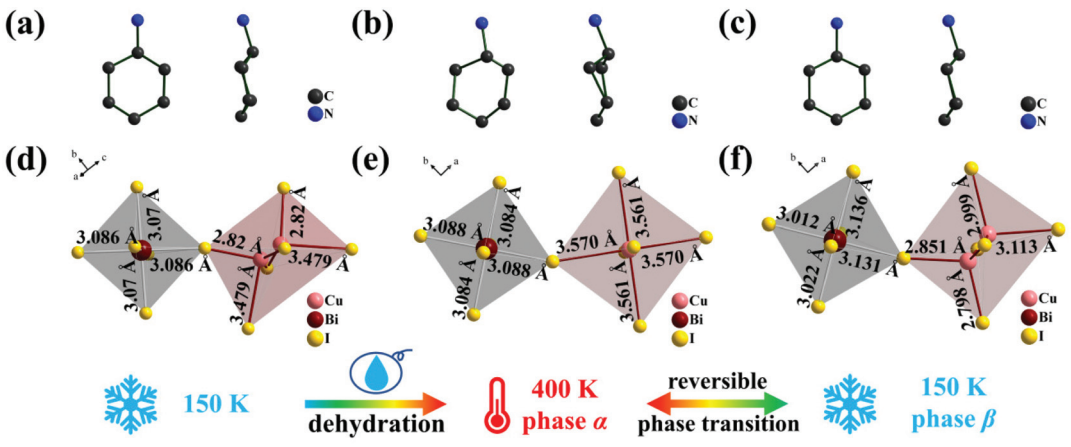

Fig. 2 Front and side views of cations of (a) $(CHA)_4CuBiI_8{\cdot}H_2O$ and $(CHA)_4CuBiI_8$ in (b) α and (c) β phases. Bond lengths of Cu-based and Bi-based octahedra of (d) $(CHA)_4CuBiI_8{\cdot}H_2O$ and $(CHA)_4CuBiI_8$ in (e) α and (f) β phases viewed perpendicular to the two-dimensional plane.

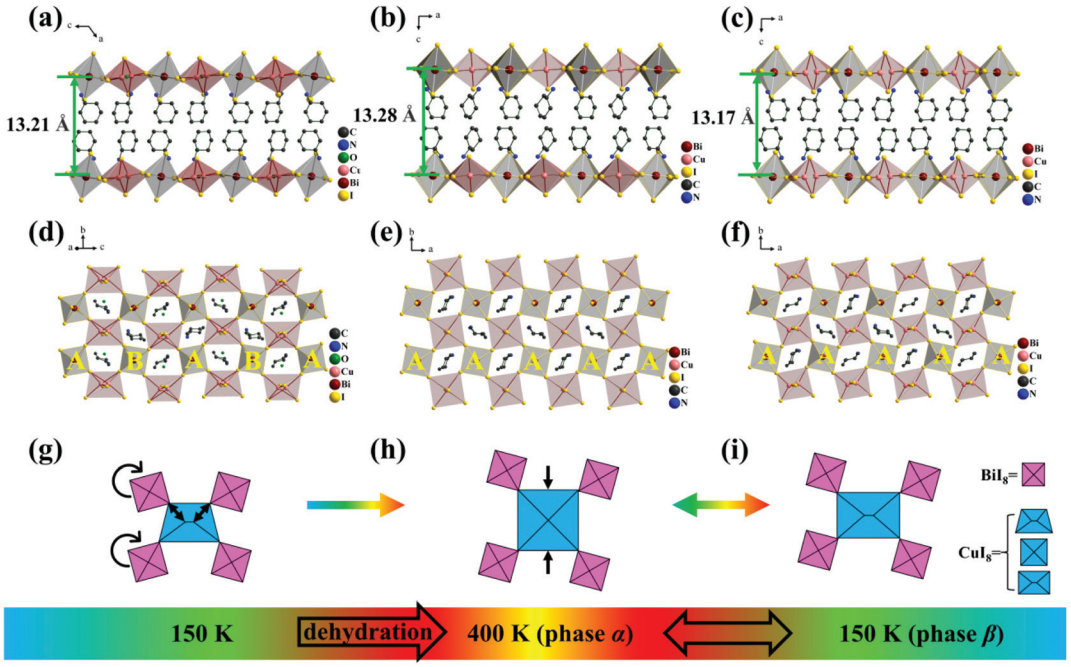

Fig. 3 (a–c) Diagram of the two-dimensional layer distance, (d–f) the bimetal skeleton structure observed perpendicular to the two-dimensional plane and a schematic diagram of the (g–i) bimetal skeleton transformation of $(CHA)_4CuBiI_8{\cdot}H_2O$ at 150 K and $(CHA)_4CuBiI_8$ in the α and β phases.

dicular to the two-dimensional plane to compare $(CHA)_4CuBiI_8{\cdot}H_2O$ at 150 K (Fig. 3d) with $(CHA)_4CuBiI_8$ at 400 K and 150 K (Fig. 3e and f), it is not difficult to find that half of the BiI_6 octahedra rotate with CuI_6 in the reference and the final structure underwent a transformation from "ABABA" to "AAAAA" after dehydration, resulting from the change in the Cu–I bond lengths parallel to the inorganic layer. Due to the restricted contribution near to the band gap of the organic part, these transformations of the spatial arrangement of the inorganic part, including the intralayer distortion and interlayer distance, are decisive factors behind the change in the UV-vis absorption of $(CHA)_4CuBiI_8{\cdot}H_2O$ and $(CHA)_4CuBiI_8$

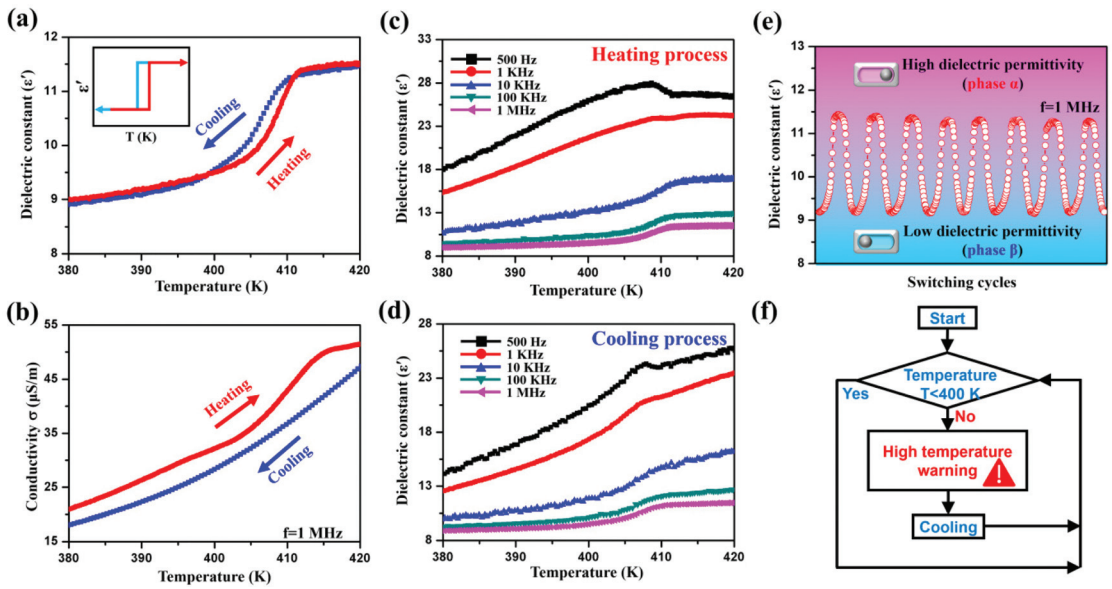

Fig. 4 (a) Dielectric constant ε' and (b) conductivity σ of $(CHA)_4CuBiI_8$ as a function of temperature. (c and d) Temperature dependence of the real part (ε') of $(CHA)_4CuBiI_8$ at different frequencies. (e) Multiple reversible switching of the dielectric constant (ε') of $(CHA)_4CuBiI_8$. (f) Logic diagram of a temperature-controlled device.

(Fig. S5, ESI†).[42] Besides this, Fig. 3g–i were constructed to better understand the transformation of the inorganic skeleton before and after dehydration.

In general, the dehydration of $(CHA)_4CuBiI_8{\cdot}H_2O$ directly changes the internal arrangement of the inorganic skeleton, resulting in the activation of the solid-to-solid structural phase transition material $(CHA)_4CuBiI_8$. For $(CHA)_4CuBiI_8$, the reason for its phase transition originates from the overall coordination between the distortion and movement of the inorganic skeleton and the thermal deformation of the cationic structure.

Temperature-dependent dielectric permittivity measurements

As reversible phase transition materials, their physical properties can respond to external stimuli, including electric and magnetic fields, pressure, temperature and light near the solid-to-solid phase transition point.[59–62] On this basis, the temperature-dependent dielectric constant ε' [the real part (ε') of the complex dielectric constant $\varepsilon = \varepsilon' - i\varepsilon''$, in which ε'' is the imaginary part] was investigated between 500 Hz and 1 MHz and the corresponding conductivity was calculated using the formula $\varepsilon'' = \varepsilon' \tan\theta$ and $\sigma_{a.c.} = \omega\varepsilon''\varepsilon_0$ (ε_0 is the permittivity of vacuum), presented in Fig. 4a and b. In both heating and cooling processes, the dielectric constant (ε') curve shows a step change at ~400 K at a frequency of 1 MHz. When applying different frequencies, the change in the dielectric constant (ε') during heating and cooling is also the same as that at a high frequency of 1 MHz (Fig. 4c and d), which is consistent with the DSC results. As a potential temperature sensing material, it was necessary to conduct phase transition stability tests. For this, multiple reversible dielectric switching tests were performed, and $(CHA)_4CuBiI_8$ showed good cycling stability (Fig. 4e). We designed a temperature sensing logic diagram based on dielectric permittivity (Fig. 4f), meaning that when the temperature exceeds 400 K, that is, the phase transition temperature, the sudden change in the dielectric/high dielectric constant gives a high-temperature warning. Otherwise, no warning is given.

Conclusions

We found that the two-dimensional hybrid perovskite material $(CHA)_4CuBiI_8{\cdot}H_2O$ can be converted into the solid-to-solid structural phase transition material $(CHA)_4CuBiI_8$ by dehydration, with the reason for its phase transition being the overall coordination of the distortion and movement of the inorganic skeleton and the thermal deformation of the cationic structure. The interesting discovery of the dehydration activation of this material provides a new idea for the discovery and potential application of more physical properties of double perovskites.

Author contributions

R.-Y. R. and C.-Y. S. conceived and conducted the experiments, analyzed the data and wrote the paper. T. S. and Z.-X. Z. carried out the dielectric characterization. P.-Z. H. and Y. Z. assisted data analysis. D.-W. F. and Q.-Q. J. guided and supervised this work.

Conflicts of interest

The authors declare no conflict of interest.

Acknowledgements

This work was financially supported by the Natural Science Foundation of Zhejiang Province (LZ20B010001) and the National Natural Science Foundation of China (NSFC 21991141).

Notes and references

1 X.-L. Xu, L.-B. Xiao, J. Zhao, B.-K. Pan, J. Li, W.-Q. Liao, R.-G. Xiong and G.-F. Zou, *Angew. Chem., Int. Ed.*, 2020, **59**, 19974–19982.
2 A. Sharenko and M. F. Toney, *J. Am. Chem. Soc.*, 2016, **138**, 463–470.
3 E. Elahi, G. Dastgeer, A. S. Siddiqui, S. A. Patil, M. W. Iqbal and P. R. Sharma, *Dalton Trans.*, 2022, **51**, 797–816.
4 M. Safdari, P. H. Svensson, M. T. Hoang, I. Oh, L. Kloo and J. M. Gardner, *J. Mater. Chem. A*, 2016, **4**, 15638–15646.
5 M. H. Futscher, J. M. Lee, L. McGovern, L. A. Muscarella, T. Wang, M. I. Haider, A. Fakharuddin, L. Schmidt-Mende and B. Ehrler, *Mater. Horiz.*, 2019, **6**, 1497–1503.
6 S. Wang, J. Fang, C. Zhang, S. Sun, K. Wang, S. Xiao and Q. Song, *Adv. Opt. Mater.*, 2017, **5**, 1700529.
7 S. Yan, K. Wang, G. Xing, J. Xu, S. Su, Z. Tang, S. Wang and K. W. Ng, *ACS Appl. Mater. Interfaces*, 2021, **13**, 38458–38466.
8 C. Zhao and C. Qin, *Nanophotonics*, 2021, **10**, 2167–2180.
9 V. Adinolfi, W. Peng, G. Walters, O. M. Bakr and E. H. Sargent, *Adv. Mater.*, 2018, **30**, 1700764.
10 W. Li, Y. Xu, J. Peng, R. Li, J. Song, H. Huang, L. Cui and Q. Lin, *ACS Appl. Mater. Interfaces*, 2021, **13**, 2971–2978.
11 K. Leng, I. Abdelwahab, I. Verzhbitskiy, M. Telychko, L. Chu, W. Fu, X. Chi, N. Guo, Z. Chen, Z. Chen, C. Zhang, Q.-H. Xu, J. Lu, M. Chhowalla, G. Eda and K. P. Loh, *Nat. Mater.*, 2018, **17**, 908–914.
12 T.-T. Sha, Y.-A. Xiong, Q. Pan, X.-G. Chen, X.-J. Song, J. Yao, S.-R. Miao, Z.-Y. Jing, Z.-J. Feng, Y.-M. You and R.-G. Xiong, *Adv. Mater.*, 2019, **31**, 1901843.
13 X.-G. Chen, X.-J. Song, Z.-X. Zhang, P.-F. Li, J.-Z. Ge, Y.-Y. Tang, J.-X. Gao, W.-Y. Zhang, D.-W. Fu, Y.-M. You and R.-G. Xiong, *J. Am. Chem. Soc.*, 2020, **142**, 1077–1082.
14 X.-G. Chen, X.-J. Song, Z.-X. Zhang, H.-Y. Zhang, Q. Pan, J. Yao, Y.-M. You and R.-G. Xiong, *J. Am. Chem. Soc.*, 2020, **142**, 10212–10218.

15 H.-Y. Zhang, X.-J. Song, X.-G. Chen, Z.-X. Zhang, Y.-M. You, Y.-Y. Tang and R.-G. Xiong, *J. Am. Chem. Soc.*, 2020, **142**, 4925–4931.
16 H.-Y. Zhang, X.-J. Song, H. Cheng, Y.-L. Zeng, Y. Zhang, P.-F. Li, W.-Q. Liao and R.-G. Xiong, *J. Am. Chem. Soc.*, 2020, **142**, 4604–4608.
17 H. Yu, H. Wang, G. Pozina, C. Yin, X.-K. Liu and F. Gao, *Chem. Sci.*, 2020, **11**, 11338–11343.
18 H. Cho, S.-H. Jeong, M.-H. Park, Y.-H. Kim, C. Wolf, C.-L. Lee, J. H. Heo, A. Sadhanala, N. Myoung, S. Yoo, S. H. Im, R. H. Friend and T.-W. Lee, *Science*, 2015, **350**, 1222–1225.
19 D. Yang, G. Zhang, R. Lai, Y. Cheng, Y. Lian, M. Rao, D. Huo, D. Lan, B. Zhao and D. Di, *Nat. Commun.*, 2021, **12**, 4295.
20 C. Su, M. Lun, Y. Chen, Y. Zhou, Z. Zhang, M. Chen, P. Huang, D. Fu and Y. Zhang, *CCS Chem.*, 2021, **3**, 2021–2031.
21 Y.-Y. Guo and P. Lightfoot, *Dalton Trans.*, 2020, **49**, 12767–12775.
22 A. Babayigit, A. Ethirajan, M. Muller and B. Conings, *Nat. Mater.*, 2016, **15**, 247–251.
23 Y. Liu, A. Nag, L. Manna and Z. Xia, *Angew. Chem., Int. Ed.*, 2021, **60**, 11592–11603.
24 U. Farooq, M. Ishaq, U. A. Shah, S. Chen, Z.-H. Zheng, M. Azam, Z.-H. Su, R. Tang, P. Fan, Y. Bai and G.-X. Liang, *Nano Energy*, 2022, **92**, 106710.
25 M. Waqar, H. Wu, J. Chen, K. Yao and J. Wang, *Adv. Mater.*, 2021, 2106845.
26 H.-Y. Zhang, X.-G. Chen, Z.-X. Zhang, X.-J. Song, T. Zhang, Q. Pan, Y. Zhang and R.-G. Xiong, *Adv. Mater.*, 2020, **32**, 2005213.
27 G.-P. Li, S.-Q. Lu, X. Chen, W.-Q. Liao, Y.-Y. Tang and R.-G. Xiong, *Chem. – Eur. J.*, 2019, **25**, 16625–16629.
28 B. Vargas, G. Rodriguez-Lopez and D. Solis-Ibarra, *ACS Energy Lett.*, 2020, **5**, 3591–3608.
29 D. Fu, S. Wu, Y. Liu, Y. Yao, Y. He and X.-M. Zhang, *Inorg. Chem. Front.*, 2021, **8**, 3576–3580.
30 L.-Y. Bi, Y.-Q. Hu, M.-Q. Li, T.-L. Hu, H.-L. Zhang, X.-T. Yin, W.-X. Que, M. S. Lassoued and Y.-Z. Zheng, *J. Mater. Chem. A*, 2019, **7**, 19662–19667.
31 Z. Xiao, Z. Song and Y. Yan, *Adv. Mater.*, 2019, **31**, 1803792.
32 H. Ruan, Z. Guo, J. Lin, K. Liu, L. Guo, X. Chen, J. Zhao, Q. Liu and W. Yuan, *Inorg. Chem.*, 2021, **60**, 14629–14635.
33 N. R. Wolf, B. A. Connor, A. H. Slavney and H. I. Karunadasa, *Angew. Chem., Int. Ed.*, 2021, **60**, 16264–16278.
34 X.-G. Zhao, D. Yang, J.-C. Ren, Y. Sun, Z. Xiao and L. Zhang, *Joule*, 2018, **2**, 1662–1673.
35 F. Igbari, Z.-K. Wang and L.-S. Liao, *Adv. Energy Mater.*, 2019, **9**, 1803150.
36 C. Shi, J.-J. Ma, J.-Y. Jiang, M.-M. Hua, Q. Xu, H. Yu, Y. Zhang and H.-Y. Ye, *J. Am. Chem. Soc.*, 2020, **142**, 9634–9641.
37 P. Vishnoi, J. L. Zuo, X. Li, D. C. Binwal, K. E. Wyckoff, L. Mao, L. Kautzsch, G. Wu, S. D. Wilson, M. G. Kanatzidis, R. Seshadri and A. K. Cheetham, *J. Am. Chem. Soc.*, 2022, **144**, 6661–6666.
38 C.-F. Wang, H. Li, M.-G. Li, Y. Cui, X. Son, Q.-W. Wang, J.-Y. Jiang, M.-M. Hua, Q. Xu, K. Zhao, H.-Y. Ye and Y. Zhang, *Adv. Funct. Mater.*, 2021, **31**, 2009457.
39 W. Guo, X. Liu, S. Han, Y. Liu, Z. Xu, M. Hong, J. Luo and Z. Sun, *Angew. Chem., Int. Ed.*, 2020, **59**, 13879–13884.
40 C. Shi, L. Ye, Z.-X. Gong, J.-J. Ma, Q.-W. Wang, J.-Y. Jiang, M.-M. Hua, C.-F. Wang, H. Yu, Y. Zhang and H.-Y. Ye, *J. Am. Chem. Soc.*, 2020, **142**, 545–551.
41 Y. Fang, L. Zhang, L. Wu, J. Yan, Y. Lin, K. Wang, W. L. Mao and B. Zou, *Angew. Chem., Int. Ed.*, 2019, **58**, 15249–15253.
42 L.-Y. Bi, T.-L. Hu, M.-Q. Li, B.-K. Ling, M. S. Lassoued, Y.-Q. Hu, Z. Wu, G. Zhou and Y.-Z. Zheng, *J. Mater. Chem. A*, 2020, **8**, 7288–7296.
43 D. Li, X. Liu, W. Wu, Y. Peng, S. Zhao, L. Li, M. Hong and J. Luo, *Angew. Chem., Int. Ed.*, 2021, **60**, 8415–8418.
44 Y. Li, T. Yang, Z. Xu, X. Liu, X. Huang, S. Han, Y. Liu, M. Li, J. Luo and Z. Sun, *Angew. Chem., Int. Ed.*, 2020, **59**, 3429–3433.
45 C. Su, Z. Zhang, J. Yao, M. Chen, P. Huang, Y. Zhang, D. Fu and L. Xie, *Chin. Chem. Lett.*, 2022, DOI: **10.1016/j.cclet.2022.04.040**.
46 Y. Yao, B. Kou, Y. Peng, Z. Wu, L. Li, S. Wang, X. Zhang, X. Liu and J. Luo, *Chem. Commun.*, 2020, **56**, 3206–3209.
47 C.-Y. Su, Y.-F. Yao, Z.-X. Zhang, Y. Wang, M. Chen, P.-Z. Huang, Y. Zhang, W.-C. Qiao and D.-W. Fu, *Chem. Sci.*, 2022, **13**, 4794–4800.
48 P. Vishnoi, R. Seshadri and A. K. Cheetham, *J. Phys. Chem. C*, 2021, **125**, 11756–11764.
49 M. S. Lassoued, L.-Y. Bi, Z. Wu, G. Zhou and Y.-Z. Zheng, *J. Mater. Chem. C*, 2020, **8**, 5349–5354.
50 A. Douangamath, P. Aller, P. Lukacik, J. Sanchez-Weatherby, I. Moraes and J. Brandao-Neto, *Acta Crystallogr., Sect. D: Biol. Crystallogr.*, 2013, **69**, 920–923.
51 Y. Yoshida, K. Inoue, K. Kikuchi and M. Kurmoo, *Chem. Mater.*, 2016, **28**, 7029–7038.
52 M. Kurmoo, H. Kumagai, K. W. Chapman and C. J. Kepert, *Chem. Commun.*, 2005, 3012–3014.
53 A. Mesbah, P. Rabu, R. Sibille, S. Lebegue, T. Mazet, B. Malaman and M. Francois, *Inorg. Chem.*, 2014, **53**, 872–881.
54 W.-Q. Liao, H.-Y. Ye, D.-W. Fu, P.-F. Li, L.-Z. Chen and Y. Zhang, *Inorg. Chem.*, 2014, **53**, 11146–11151.
55 H.-Y. Ye, W.-Q. Liao, C.-L. Hu, Y. Zhang, Y.-M. You, J.-G. Mao, P.-F. Li and R.-G. Xiong, *Adv. Mater.*, 2016, **28**, 2579–2586.
56 Y. Wang, S. Han, X. Liu, Z. Wu, Z. Sun, D. Dey, Y. Li and J. Luo, *RSC Adv.*, 2020, **10**, 17492–17496.
57 W.-X. Chai, L.-M. Wu, J.-Q. Li and L. Chen, *Inorg. Chem.*, 2007, **46**, 8698–8704.
58 J. Moebs, M. Gerhard and J. Heine, *Dalton Trans.*, 2020, **49**, 14397–14400.

59 T. Shao, R.-Y. Ren, P.-Z. Huang, H.-F. Ni, C.-Y. Su, D.-W. Fu, L.-Y. Xie and H.-F. Lu, *Dalton Trans.*, 2022, **51**, 2005–2011.
60 Z.-X. Zhang, C.-Y. Su, J. Li, X.-J. Song, D.-W. Fu and Y. Zhang, *Chem. Mater.*, 2021, **33**, 5790–5799.
61 Y. Xie, Y. Ai, Y.-L. Zeng, W.-H. He, X.-Q. Huang, D.-W. Fu, J.-X. Gao, X.-G. Chen and Y.-Y. Tang, *J. Am. Chem. Soc.*, 2020, **142**, 12486–12492.
62 D.-W. Fu, J.-X. Gao, W.-H. He, X.-Q. Huang, Y.-H. Liu and Y. Ai, *Angew. Chem., Int. Ed.*, 2020, **59**, 17477–17481.